Indian Journal of Experimental Biology
Vol. 63, November 2025, pp. 913-927
DOI: 10.56042/ijeb.v63i11.20261

Green synthesis and characterization of silver nanoparticles using *Vitex leucoxylon* extracts: Analysis of anti-inflammatory activity

Vishnu Sravanthi M[1,2] & Nirmala S[3*]

[1]Department of Pharmaceutical Chemistry, Faculty of Pharmacy, Bharath Institute of Higher Education and Research, Chennai, India

[2]Department of Pharmaceutical Chemistry, East Point College of Pharmacy, Bangalore, India

[3]Department of Pharmacognosy, Faculty of Pharmacy, Bharath Institute of Higher Education and Research, Chennai, India

Received 02 June 2025; revised 08 September 2025

In this investigation, silver nanoparticles (AgNPs) were synthesised through an eco-friendly approach using aqueous leaf extracts of *Vitex leucoxylon*, and their anti-inflammatory activity was examined *in vitro*. The resulting nanoparticles underwent thorough physicochemical characterization employing UV–Vis spectrometry, FTIR, scanning electron microscopy, X-ray diffraction, and dynamic light scattering. A sharp absorbance near 400 nm in the UV–Vis spectrum verified successful nanoparticle formation. FTIR analysis suggested that bioactive plant compounds played a crucial role in reducing and stabilizing the silver ions. Microscopy revealed that the particles were predominantly spherical with moderate uniformity, while crystallinity was affirmed by XRD. The particles ranged in size from approximately 10 to 80 nm, and DLS analysis revealed a dual-modal distribution with peaks around 75.9 nm and 274.5 nm, along with a zeta potential of –1.3 mV. The anti-inflammatory efficacy was validated using LPS-stimulated RAW 264.7 macrophages in MTT and nitric oxide assays, showing that AgNPs enhanced cell survival and reduced nitric oxide production more effectively than the crude extract. Molecular docking studies further revealed a strong interaction between AgNPs and the COX-2 enzyme, with a binding score of –8.2 kcal/mol. These results suggest that *Vitex leucoxylon*-based AgNPs hold promise as bioactive agents in anti-inflammatory therapy.

Keywords: Phytochemical capping agents, Cyclooxygenase-2 inhibition, Nitric oxide suppression, Molecular docking proxy model, RAW 264.7 macrophages

Inflammation represents a multifaceted physiological reaction triggered by the presence of harmful agents like microbes, injured cells, or irritants[1]. Although it is a protective mechanism essential for tissue repair and healing, chronic or uncontrolled inflammation is implicated in a wide spectrum of human diseases, including rheumatoid arthritis, cardiovascular disorders, neurodegenerative conditions, diabetes mellitus, and certain types of cancer[2]. According to the World Health Organization (WHO), non-communicable diseases (NCDs) associated with chronic inflammation account for over 70% of global deaths annually. In India alone, inflammatory conditions such as arthritis affect approximately 15% of the population, while cardiovascular and metabolic disorders continue to rise due to sedentary lifestyles, dietary factors, and genetic predispositions[3]. Conventional anti-inflammatory drugs, including non-steroidal anti-inflammatory drugs (NSAIDs) and corticosteroids, are widely used to manage symptoms. However, their long-term use often leads to adverse effects such as gastrointestinal ulcers, liver damage, and immunosuppression. These limitations underscore the need for alternative, safer therapeutic agents derived from natural sources with fewer side effects and sustainable production methods[4].

Nanotechnology has emerged as a transformative field, offering novel solutions across medicine, materials science, and environmental applications[5]. Among the most widely explored nanoparticles, silver nanoparticles (AgNPs) stand out for their potent antimicrobial, antioxidant, and anti-inflammatory activities[6,7]. Traditionally, AgNPs are synthesised through physical or chemical routes that often involve hazardous reagents, high score input, and complex protocols[8]. As a sustainable alternative, green synthesis methods have gained prominence due to their simplicity, cost-effectiveness, and eco-friendliness[9].

To date, numerous plants, including *Azadirachta indica*, *Ocimum sanctum*, and *Vitex negundo,* have

*Correspondence:
E-mail: nirmala.pharm@bharathuniv.ac.in

been employed for the biogenic synthesis of AgNPs; however, *Vitex leucoxylon* (voucher number 0689) remains largely unexplored despite its established ethnopharmacological relevance. The phytochemical richness of *V. leucoxylon* particularly its abundance of flavonoids, tannins, and phenolic acids provides a unique reducing and stabilizing potential that distinguishes it from other plant sources. Moreover, its traditional use in inflammatory disorders offers a strong biological rationale for testing the therapeutic relevance of its derived nanoparticles[10,11]. Although no prior studies have reported AgNPs synthesis specifically from *V. leucoxylon*, related species such as *V. negundo* and *V. trifolia* have been documented to successfully generate stable, bioactive AgNPs, suggesting that the phytochemicals of *V. leucoxylon* are similarly effective in nanoparticle biosynthesis. To the best of our knowledge, this is the first comprehensive report on the green synthesis, characterization, and anti-inflammatory evaluation (both *in vitro* and *in silico*) of AgNPs synthesized from *V. leucoxylon*.

Materials and Methods

Preparation of plant extract

The plant was collected and authenticated by Dr. K. Madhava Chetty, Plant Taxonomist (IAAT: 337). The herbarium was recorded with voucher number 0689. Fresh leaves of *Vitex leucoxylon* were collected, thoroughly washed with distilled water to remove surface impurities, and then air-dried under shade to retain their phytochemical properties. A total of 10 g of the cleaned plant material was finely chopped and subjected to Soxhlet extraction for a duration of 24 hours (3 cycles) using water as solvent. The temperature was maintained around 45°C throughout the extraction process. In this study, the extraction of bioactive constituents from the plant material into water was achieved through a heat-assisted process. Once the boiling step was completed, the solution was left to cool naturally to ambient temperature. It was then subjected to filtration using Whatman no. 1 filter paper to remove remaining solid plant particles. The resulting clear filtrate, rich in phytoconstituents, was collected and stored at 4 °C for further use in the synthesis of silver nanoparticles[12].

Phytochemical analysis

Qualitative phytochemical analysis was conducted by using Pandey *et al*. procedure with minor modifications. "*V. leucoxylon* was qualitatively tested for the presence of various phytochemical constituents such as flavonoids, alkaloids, phenols, glycosides, sterols, lignins, saponins, anthraquinones, tannins, and reducing sugars"[13].

Preparation of silver nitrate solution

To prepare the $AgNO_3$ solution, a modified method based on Liaqat *et al*. was followed[14]. A 5 mM solution of $AgNO_3$ was freshly prepared by dissolving the appropriate amount of the compound in distilled water. The solution was kept in a light-protected container to prevent degradation and stored under dark conditions until required for nanoparticle synthesis.

Green synthesis of silver nanoparticles

The aqueous extract of *Vitex leucoxylon* leaves was heated to 60 °C and maintained at this temperature for about 30 minutes to activate phytochemicals and enhance their reducing properties. An equal volume (50 mL) of this extract was then combined with 50 mL of the 5 mM $AgNO_3$ solution in a 1:1 ratio under constant stirring. The reaction mixture was kept at a stable temperature ranging between 60–70 °C for 30 minutes to facilitate the bioreduction process. A distinct colour change from pale yellow to deep brown indicated the successful conversion of silver ions (Ag^+) into metallic silver nanoparticles (Ag^0). This visual transformation was attributed to surface plasmon resonance (SPR), a hallmark of silver nanoparticle synthesis[15]. The pH of the reaction mixture remained nearly neutral (6.8–7.2) without adjustment, which allowed phytochemicals such as flavonoids and phenols to function effectively as reducing and stabilising agents.

Purification and drying

Upon completion of the reaction, the colloidal suspension containing AgNPs was subjected to centrifugation at 10,000 rpm for 15 minutes to pellet the nanoparticles. The resultant pellet was washed multiple times with distilled water and ethanol to remove residual plant biomolecules and unreacted silver ions. The purified nanoparticles were then dried in a hot-air oven at 50 °C for 24 to 48 hours. For further enhancement of stability and surface capping, the dried nanoparticle powder was calcined in a muffle furnace at temperatures ranging between 400 °C and 500 °C[16].

Characterization of silver nanoparticles

The synthesized AgNPs were subjected to comprehensive physicochemical characterization using a combination of analytical techniques to confirm their formation, determine structural and morphological attributes, and evaluate their size distribution. The characterization was conducted by using Nahari *et al.* procedure with minor modification[17].

UV–Visible spectroscopy analysis

The initial confirmation of silver nanoparticle synthesis was obtained using UV-Vis spectrophotometry. The optical absorption spectrum of the colloidal solution was recorded in the wavelength range of 300 to 700 nm. The intensity and sharpness of the peak provided preliminary evidence of nanoparticle formation and indicated a relatively narrow size distribution.

Fourier Transform Infrared Spectroscopy (FTIR) analysis

FTIR spectroscopy was conducted to evaluate possible functional regions of the plant extract as well as the nanoparticles. The spectra were recorded using an FTIR (Shimadzu IR Affinity-1) operating in the 4000–400 cm^{-1} wavelength range.

X-ray diffraction (XRD) analysis

The X-ray diffraction method was used to determine the crystalline structure and phase purity of the nanoparticles over a 2θ range of 20° to 80°. The diffractogram exhibited well-defined peaks at 2θ values was used to confirm the nature of metallic silver. The average crystallite size was calculated using the Debye-Scherrer equation, and it was found to be in the nanometer range, further validating the successful synthesis of AgNPs.

Scanning Electron Microscopy (SEM)

The surface morphology and topographical features of the synthesised silver nanoparticles were examined using SEM. The micrographs revealed predominantly spherical particles with relatively uniform size and distribution. The images indicated minimal agglomeration, suggesting effective capping by phytochemicals present in the *Vitex leucoxylon* extract. The SEM images also supported the structural integrity of the nanoparticles even after calcination[18].

Dynamic Light Scattering (DLS) analysis

The hydrodynamic diameter and size distribution profile of the AgNPs in colloidal form were determined by the DLS method. The polydispersity index (PDI), particle size distribution, and zeta potential measurement confirmed that the nanoparticles possessed a negative surface charge, reflecting good colloidal stability likely due to the capping action of the bioactive compounds in the plant extract.

Evaluation of anti-inflammatory activity

LPS induced anti-inflammatory assay using RAW 264.7 cells

The anti-inflammatory potential of the biosynthesised silver nanoparticles (AgNPs) using *V. leucoxylon* extract was evaluated through a lipopolysaccharide (LPS)-induced inflammatory model in RAW 264.7 murine macrophage cells. RAW 264.7 cells were selected as they are a well-established model for inflammation studies: upon LPS stimulation, they secrete nitric oxide and pro-inflammatory cytokines through iNOS activation, making them highly relevant for screening anti-inflammatory effects of natural products and nanoparticles[19]. The assay measured cell recovery following LPS-induced inflammation and subsequent treatment with varying concentrations of AgNPs, using the MTT assay as an indicator of cell viability.

Cell preparation and seeding

"RAW 264.7 cells were cultured and adjusted to a concentration of 1.0×10^5 cells/mL. A total of 50,000 cells per well were seeded into sterile 96-well culture plates and incubated for 24 hours at 37 °C in a humidified atmosphere containing 5% CO_2 to allow cell adherence and stabilisation"[20].

Induction of inflammatory response

Following the incubation period, inflammation was induced by adding 80 ng/mL of LPS to each well. The plates were further incubated for 4 hours under the same conditions to stimulate an inflammatory response, simulating immune activation.

Treatment with biosynthesised nanoparticles

After LPS induction, the medium in each well was carefully aspirated and replaced with 100 µL of various test concentrations (10-320 ng/mL for VL extract, 1.25-80 ng/mL for AgVL extract) of the biosynthesised AgNPs. The treated plates were then incubated for an additional 24 hours at 37 °C in a 5% CO_2 environment, allowing sufficient exposure for potential anti-inflammatory effects[21].

MTT assay and absorbance measurement

To assess the viability and proliferation of cells, the culture medium was gently discarded following the incubation period. Subsequently, 100 µL of MTT reagent, prepared by dissolving 5 mg of MTT in 10 mL of phosphate-buffered saline, was added to each well. The plates were then incubated for 4 hours, allowing metabolically active cells to reduce MTT into insoluble formazan crystals. After incubation, the supernatant was carefully removed, and 100 µL of dimethyl sulfoxide (DMSO) was added to each well to dissolve the resulting crystals. The absorbance was then measured at 590 nm using a microplate reader. The percentage of cell recovery, reflecting the anti-inflammatory effect, was calculated as per the formula provided in Equation 1.

$$Recovery\ (\%) = 100 - (\frac{OD\ of\ Sample}{OD\ of\ Control}) \times 100$$

This calculation allowed for the quantification of inflammation reversal or inhibition in response to nanoparticle treatment. A higher recovery percentage indicated a greater anti-inflammatory effect exerted by the silver nanoparticles[22].

Nitric oxide (NO) assay

Materials and cell culture

To investigate the anti-inflammatory activity of AgNPs synthesised from *Vitex leucoxylon* extracts, a nitric oxide assay was performed using RAW 264.7 murine macrophage cells. These cells were maintained in Dulbecco′s Modified Eagle Medium (DMEM) enriched with 10% heat-inactivated fetal bovine serum (FBS), along with antibiotics penicillin (100 IU/mL) and streptomycin (100 µg/mL). Cultures were incubated at 37°C in a 5% CO_2 humidified environment. Once the cells reached confluency, they were sub-cultured using TPVG dissociation solution, comprising 0.2% trypsin, 0.02% EDTA, and 0.05% glucose in phosphate-buffered saline (PBS). Before initiating the experiment, cell viability was confirmed, and viable cells were collected by centrifugation for further analysis[23].

Assay procedure

"The cells were diluted to a final concentration of 1.0×10^5 cells/mL and seeded at a density of 50,000 cells per well in 96-well flat-bottom microtiter plates. Plates were incubated for 24 hours at 37 °C in a 5% CO_2 environment to allow proper adherence and stabilisation of the cell monolayer. Inflammation was induced by adding 80 ng/mL of LPS to each well. LPS-treated plates were incubated for 4 hours to stimulate nitric oxide production via inducible nitric oxide synthase (iNOS) activation. Following this, 100 µL of varying concentrations of the biosynthesised AgNPs was added to the respective wells. The plates were incubated for an additional 24 hours under standard culture conditions"[24].

After the treatment period, cells were harvested by gentle trypsinization and centrifugation, followed by resuspension in plain culture medium. The cell suspensions were homogenized lightly to ensure uniform distribution, and 100 µL of each sample was transferred into fresh wells. Then, 100 µL of freshly prepared Griess reagent (filtered through a 0.2 µm membrane and stored at 2–8 °C) was added to each well to react with the nitrite, a stable end-product of nitric oxide. The plates were incubated for 1 hour at 37 °C. The absorbance was measured at 540 nm using a microplate reader. Nitric oxide concentration was quantified by constructing a standard curve using sodium nitrite and applying linear regression to derive the nitrite concentration in each test sample. A decrease in NO production compared to the LPS control indicated the anti-inflammatory potential of the test nanoparticles[25].

***In silico* study**

An *in silico* molecular docking study was performed to assess the potential anti-inflammatory interaction of plant-extract-mediated AgNPs by modeling them using a dummy metal, zinc (Zn), due to AutoDock Vina′s limitations in accurately simulating metallic nanoparticles (Fig. 1). Cyclooxygenase-2 (COX-2), a key pro-inflammatory enzyme, was selected as the target protein, and its three-dimensional crystal structure was obtained from the RCSB Protein Data Bank (PDB ID: 3LN1)[7].

The protein structure was preprocessed using AutoDock Tools (version 1.5.7). All heteroatoms,

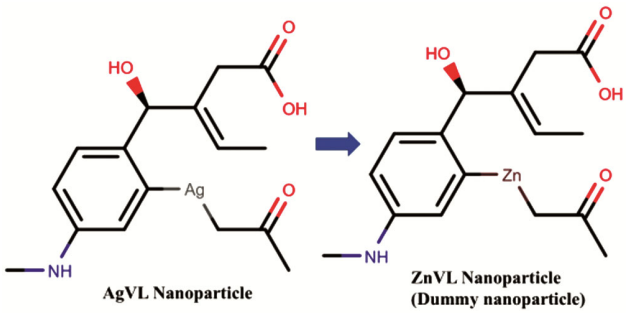

Fig. 1 — 2D structure of AgVL nanoparticle and ZnVL dummy nanoparticle.

including water molecules and the co-crystallized inhibitor, were removed. Polar hydrogen atoms were added, and Kollman charges were assigned. The cleaned and processed protein structure was saved in PDBQT format, which is compatible with AutoDock Vina v1.2.0[26]. For the ligand, a zinc-based model was designed to represent the core of silver nanoparticles, simulating its potential coordination behaviour with the active site residues of COX-2. The Zn atom was manually incorporated into a simple organic scaffold derived from dominant phytochemicals identified from FTIR spectra of the plant extract (e.g., flavonoids or phenolic acids). The structure was built using Avogadro software and optimized using the MMFF94 force field. The geometry-optimized ligand structure was then converted to PDB format after assigning Gasteiger charges[27].

Molecular docking simulations were carried out using the online web server CB-DOCK 2 (https://cadd.labshare.cn/cb-dock2/index.php). CB-DOCK 2 utilised the AutoDock Vina model and performed the simulation. The PDB file of protein and ligand was uploaded to the server interface. CB-DOCK 2 automatically selected the binding pocket, grid box, and dimension around the co-crystal ligand[28]. All the parameters were used as default, and docking simulation was performed (Table 1). AutoDock Vina returned multiple binding poses ranked by binding affinity in kcal/mol. The pose with the lowest score was selected for interaction analysis. The visualised result was obtained from the CB-DOCK 2. The interactions between the Zn-based ligand and the active site residues of COX-2 were carefully examined. Notable interactions such as hydrogen bonding, metal coordination, and hydrophobic contacts were identified, which are known to play significant roles in ligand binding and inhibition.

Statistical analysis

The results were presented in percentage recovery/inhibition (*in vitro*) and kcal/mol (*in silico*).

Results

Extraction and phytochemical analysis

The yield of ethanolic extract was found to be 4.1%. Qualitative phytochemical screening of *V. leucoxylon* extract confirmed the presence of flavonoids, phenols, tannins, and saponins, which are widely recognised as natural reducing and stabilising agents in green nanoparticle synthesis. Although advanced chemical profiling methods such as LC–MS or GC–MS were not employed in this study, the FTIR spectra further corroborated the involvement of these functional groups in nanoparticle formation.

UV–visible spectroscopy analysis

The formation and optical behaviour of biosynthesised AgNPs using *Vitex leucoxylon* extract were confirmed through UV–Visible spectroscopy. As shown in Fig. 2, the absorption spectrum exhibited a well-defined peak at 400 nm, which is characteristic of the SPR of spherical silver nanoparticles.

This SPR band arises due to the collective oscillation of conduction electrons in response to incident light, and its presence around 400 nm is a strong indication of the successful synthesis of AgNPs. The sharpness and symmetry of the peak suggest a relatively narrow particle size distribution and good monodispersity. The absence of additional peaks in the visible range also implies minimal aggregation and supports the stability of the colloidal nanoparticle suspension. The observed peak position further indicates that the nanoparticles are likely in the size range of 10–80 nm, consistent with reported values for AgNPs synthesised via plant-mediated green synthesis routes. These findings corroborate the visual colour change observed during synthesis and provide an initial confirmation of nanoparticle formation.

FTIR analysis

FTIR spectroscopy was performed to identify the functional groups in *Vitex leucoxylon* extract that were responsible for the reduction and capping of silver ions in the formation of AgNPs. Fig. 3 shows the comparative FTIR spectra of biosynthesised $AgNO_3$VL and pure silver nitrate.

The FTIR spectrum of $AgNO_3$ VL exhibited a broad and prominent peak at ~3200 cm^{-1}, indicative of O–H stretching vibrations, typically associated with phenolic and hydroxyl groups. These phytochemical moieties likely played a major role in reducing Ag^+ to Ag^0. Strong peaks observed at 1619 cm^{-1}, 1604 cm^{-1}, and 1644 cm^{-1} correspond to C=C stretching of aromatic rings and C=O stretching of amide or ketone groups, suggesting the involvement of flavonoids, tannins, and proteins in nanoparticle formation and stabilisation. Additional bands at 1506–1394 cm^{-1} and 1334–1218 cm^{-1} represent N–O stretching of nitro compounds and C–N stretching of amines or proteins, which are common in plant-

Table 1 — Grid box dimension and active site amino acids

Active Site	Active site coordinate	Active site amino acids
C1	Center_x = 42.152 Center_y = -40.665 Center_z = 58.559 Size_x = 35 Size_y =35 Size_z = 35	PRO:114:C,TRP:125:C,PHE:128:C,SER:129:C,LEU:131:C,LEU:210:C,GLY:211:C,HIS:212:C,GLY:213:C,VAL:214:C,ASP:215:C,TYR:359:C,GLN:360:C,ASN:361:C,ARG:362:C,GLY:519:C,GLY:522:C,ASN:523:C,PRO:524:C,SER:112:D,PRO:113:D,PRO:114:D,TRP:125:D,PHE:128:D,SER:129:D,ASN:130:D,LEU:131:D,LEU:210:D,GLY:211:D,HIS:212:D,GLY:213:D,ASP:215:D,TYR:359:D,GLN:360:D,ASN:361:D,ARG:362:D,GLY:519:D,GLY:522:D,ASN:523:D,PRO:524:D
C2	Center_x = 70.324 Center_y = -36.459 Center_z = -17.684 Size_x = 29 Size_y =35 Size_z = 21	GLU:308:A,TRP:309:A,GLN:313:A,GLN:529:A,LYS:532:A,ASN:19:B,PRO:20:B,CYS:21:B,CYS:22:B,SER:23:B,ASN:24:B,PRO:25:B,CYS:26:B,GLN:27:B,ASN:28:B,ARG:29:B,GLY:30:B,GLU:31:B,CYS:32:B,MET:33:B,SER:34:B,ASP:111:B,THR:115:B,TYR:116:B,VAL:118:B,HIS:119:B,TYR:120:B,GLY:121:B,TYR:122:B,LYS:123:B,ALA:137:B,LEU:138:B,PRO:139:B,PRO:140:B,VAL:141:B,ALA:142:B,ASP:143:B,ASP:144:B,CYS:145:B,GLN:447:B,GLU:451:B,LYS:454:B,ARG:455:B
C3	Center_x = 45.642 Center_y = -14.615 Center_z = -0.340 Size_x = 35 Size_y =28 Size_z = 35	ASN:19:A,CYS:21:A,CYS:22:A,SER:23:A,ASN:24:A,PRO:25:A,CYS:26:A,GLN:27:A,ASN:28:A,ARG:29:A,GLY:30:A,GLU:31:A,CYS:32:A,MET:33:A,SER:34:A,ASP:111:A,THR:115:A,TYR:116:A,TYR:120:A,GLY:121:A,TYR:122:A,ALA:137:A,LEU:138:A,PRO:139:A,PRO:140:A,VAL:141:A,ALA:142:A,CYS:145:A,GLY:150:A,GLN:447:A,GLU:451:A,TYR:452:A,LYS:454:A,ARG:455:A,GLU:308:B,TRP:309:B,GLN:313:B,GLN:529:B,LYS:532:B
C4	Center_x = 68.008 Center_y = -50.705 Center_z = 44.632 Size_x = 21 Size_y =35 Size_z = 21	LEU:67:C,LYS:68:C,PRO:69:C,THR:70:C,PRO:71:C,ASN:72:C,VAL:74:C,HIS:75:C,THR:79:C,HIS:80:C,TYR:101:C,VAL:102:C,SER:105:C,ARG:106:C,TYR:108:C,LEU:109:C,PRO:177:C,GLN:178:C,GLY:179:C,TYR:334:C,VAL:335:C,GLN:336:C,HIS:337:C,LEU:338:C,SER:339:C,GLY:340:C,TYR:341:C,HIS:342:C,LEU:345:C,PHE:367:C,LEU:370:C,TYR:371:C,TRP:373:C,ARG:453:C,PHE:456:C,SER:457:C,LYS:459:C,TYR:461:C,GLU:466:C,LEU:467:C,GLU:496:C,LYS:497:C,PRO:498:C,ARG:499:C,PRO:500:C,ASP:501:C,ALA:502:C,ILE:503:C,PHE:504:C,GLY:505:C,GLU:506:C,THR:507:C,MET:508:C,VAL:509:C,GLU:510:C,GLY:512:C,ALA:513:C,SER:516:C,LEU:517:C,ASN:567:C 5 3967 28.597 -16.976 -17.240 21 28 21
C5	Center_x = 28.597 Center_y = -16.976 Center_z = -17.240 Size_x = 21 Size_y =28 Size_z = 21	LEU:67:A,LYS:68:A,PRO:69:A,THR:70:A,PRO:71:A,VAL:74:A,HIS:75:A,MET:99:A,TYR:101:A,VAL:102:A,LEU:103:A,SER:105:A,ARG:106:A,TYR:108:A,LEU:109:A,GLN:178:A,VAL:330:A,ILE:331:A,TYR:334:A,VAL:335:A,LEU:338:A,SER:339:A,GLY:340:A,TYR:341:A,LEU:345:A,PHE:367:A,LEU:370:A,TYR:371:A,TRP:373:A,PHE:456:A,SER:457:A,ARG:499:A,ALA:502:A,ILE:503:A,PHE:504:A,MET:508:A,VAL:509:A,GLU:510:A,LEU:511:A,GLY:512:A,ALA:513:A,PRO:514:A,SER:516:A,LEU:517:A,LEU:520:A

derived biomolecules. These peaks support the hypothesis that plant-derived proteins may act as stabilising or capping agents. A peak at 1071 cm^{-1} is attributed to C–O stretching of alcohols, ethers, or carboxylic acids, while smaller peaks between 965 cm^{-1} and 519 cm^{-1} signify bending vibrations of C–H, C–Cl, or Ag–O bonds, indicating successful interaction between silver ions and the phytochemicals.

Compared to the FTIR spectrum of pure silver nitrate (blue trace in Fig. 3), the spectrum of $AgNO_3$ VL (black trace) showed significant shifts and the emergence of new peaks, which confirm the complexation and bioreduction process. The disappearance or weakening of nitrate-associated peaks and the emergence of biologically relevant peaks further verify the successful conversion of Ag^{+} to Ag^{0} by the plant extract.

SEM analysis

The surface morphology and microstructural features of the biosynthesised AgNPs were investigated using SEM. Fig. 4 displays SEM micrographs of $AgNO_3$ VL samples at two different magnifications, revealing the overall shape, dispersion, and aggregation behaviour of the synthesised nanoparticles. The images clearly show a dense population of predominantly spherical nanoparticles. The nanoparticles appear to be moderately well-dispersed, although some degree of agglomeration is visible. This clustering may be attributed to drying during sample preparation or partial surface charge interactions among nanoparticles.

At higher magnification, the images reveal a uniform distribution of spherical and quasi-spherical particles with smooth surfaces, consistent with green

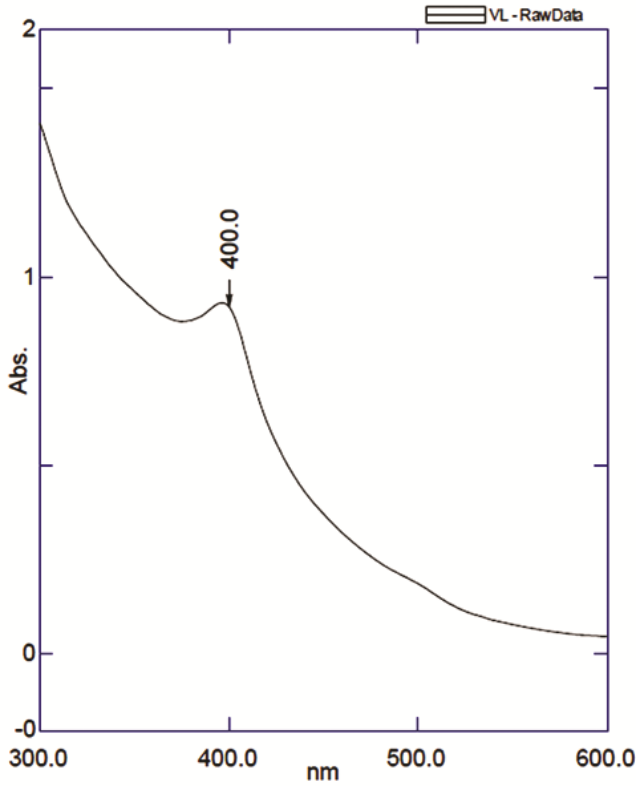

Fig. 2 — UV–Visible spectrum of AgNPs synthesized using *Vitex leucoxylon* extract, showing a characteristic SPR peak at 400 nm.

synthesised AgNPs. The morphology suggests that the phytochemicals present in *Vitex leucoxylon* extract played a dual role in reducing silver ions and stabilising the nanoparticles to prevent excessive aggregation. The average particle size visually estimated from the SEM images falls within the 10–80 nm range, which aligns well with the UV–Vis and FTIR interpretations. The presence of some larger structures may indicate secondary aggregation or incomplete capping, but the overall morphology supports successful nanoparticle synthesis via the green route.

XRD analysis

The crystalline structure and average crystallite size of the biosynthesised AgNPs using *Vitex leucoxylon* were evaluated by XRD. The XRD pattern, presented in Fig. 5, reveals a series of sharp, well-defined peaks between 2θ = 27.6° and 76.6°, confirming the crystalline nature of the synthesised nanoparticles.

Peak identification and interpretation

The XRD profile shows prominent diffraction peaks at 2θ values of 27.68°, 32.07°, 46.06°, 54.63°, 57.29°, 67.26°, 74.33°, and 76.57°. These peaks correspond to the characteristic planes of FCC silver.

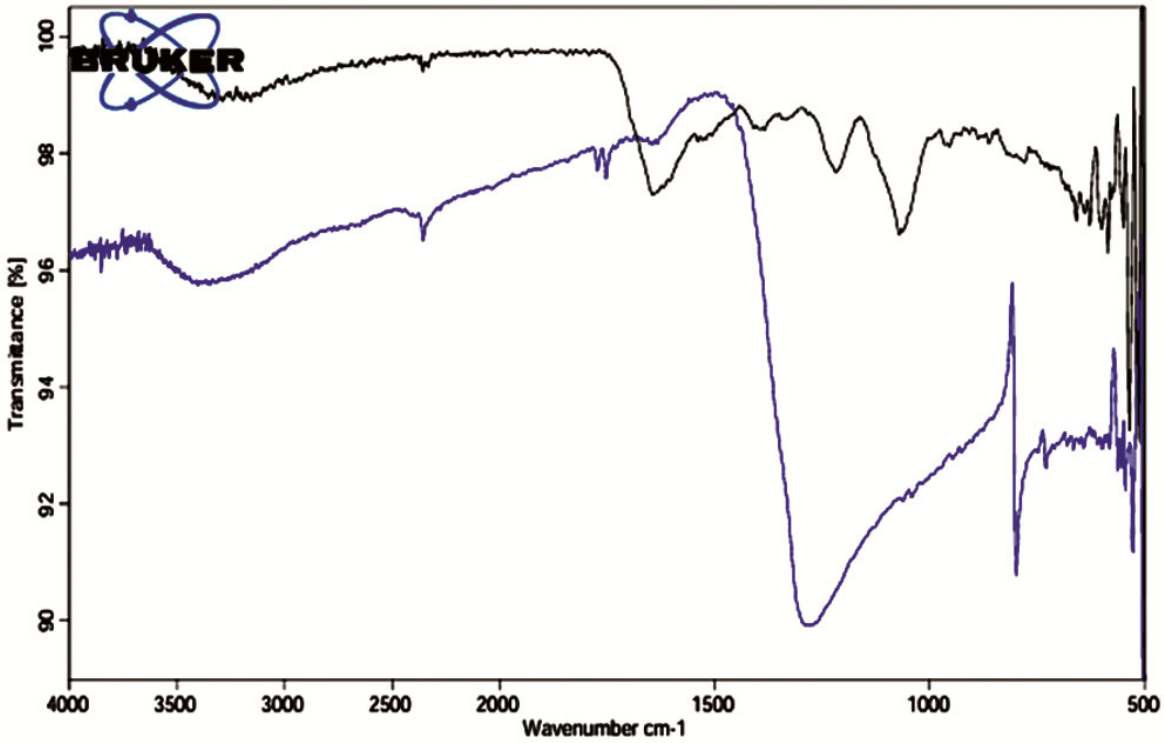

Fig. 3 — FTIR spectra of AgNPs compared to pure silver nitrate, identifying key functional groups responsible for reduction and stabilisation.

Even though the exact chemical formulae of the detected peaks were not determined, the positions, symmetry, and sharpness of the peaks confirm the high crystallinity of the nanoparticles. The intense reflection at 32.07° (highest relative intensity) suggests a dominant crystallographic plane, likely (111), typical in green synthesised AgNPs.

Crystallite size estimation

The average crystallite sizes were calculated using the Debye-Scherrer equation based on Full Width at Half Maximum (FWHM) values. As shown in the peak list, particle sizes ranged from 419 Å to 664 Å (i.e., 41.9–66.4 nm), consistent with SEM and UV–Visible observations. The relatively narrow FWHM and high peak intensity reflect a stable, well-defined nanocrystalline structure.

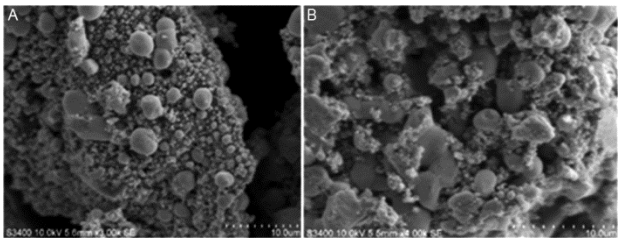

Fig. 4 — SEM micrographs of synthesised silver nanoparticles ($AgNO_3$-VL) at different magnifications, showing spherical morphology and moderate aggregation.

DLS and Zeta potential analysis

DLS was employed to evaluate the hydrodynamic size distribution and colloidal behaviour of biosynthesised AgNPs derived from *Vitex leucoxylon* extract. The DLS profile is shown in Fig. 6, with accompanying zeta potential and distribution metrics. The zeta potential was measured at −1.3 mV, which is below the conventional threshold for electrostatic stabilisation (±30 mV). Although this suggests limited electrostatic repulsion, the observed stability of the colloidal suspension may be attributed to steric stabilisation imparted by phytochemicals from the *V. leucoxylon* extract, as supported by FTIR evidence of surface-bound functional groups.

Particle size distribution

The DLS histogram revealed a bimodal particle size distribution, with two distinct populations. The primary peak was observed at 75.9 nm, comprising

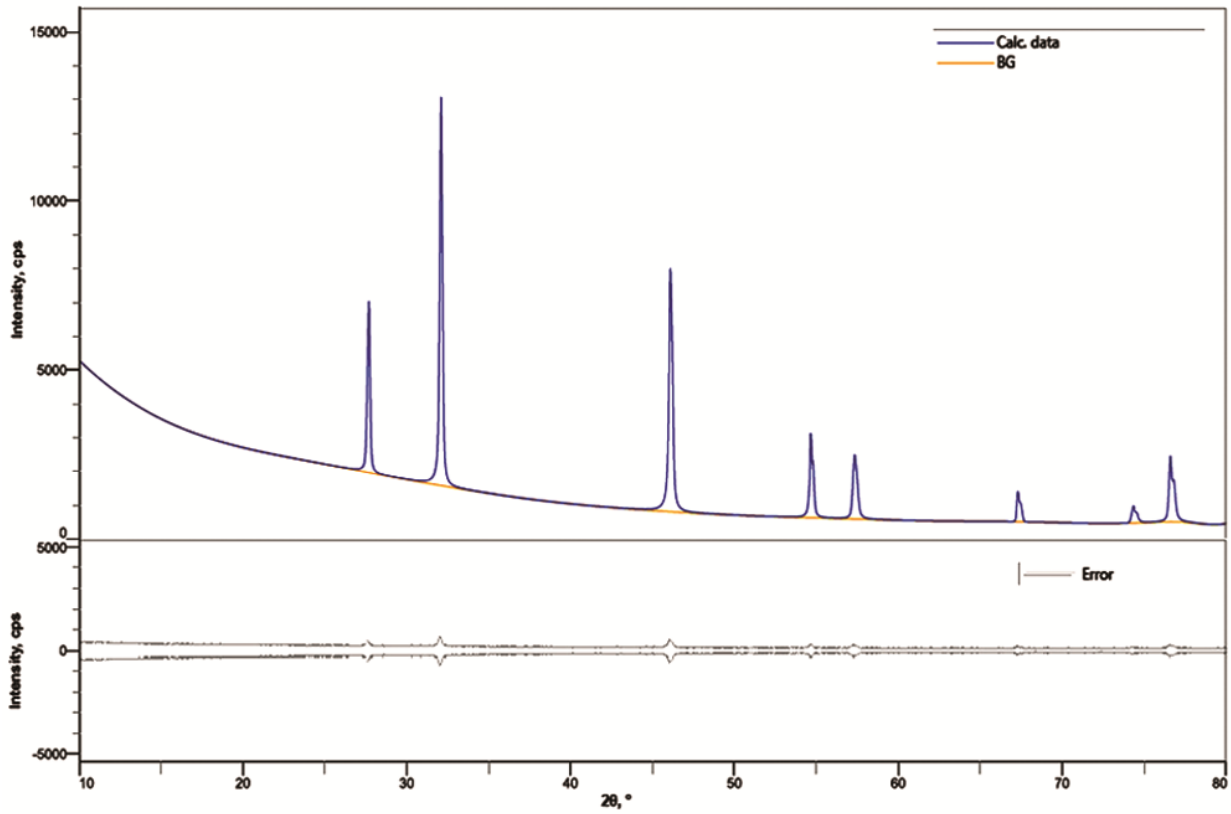

Fig. 5 — X-ray diffraction (XRD) pattern of $AgNO_3$-VL nanoparticles indicating crystallinity; peak values correspond to FCC silver structure.

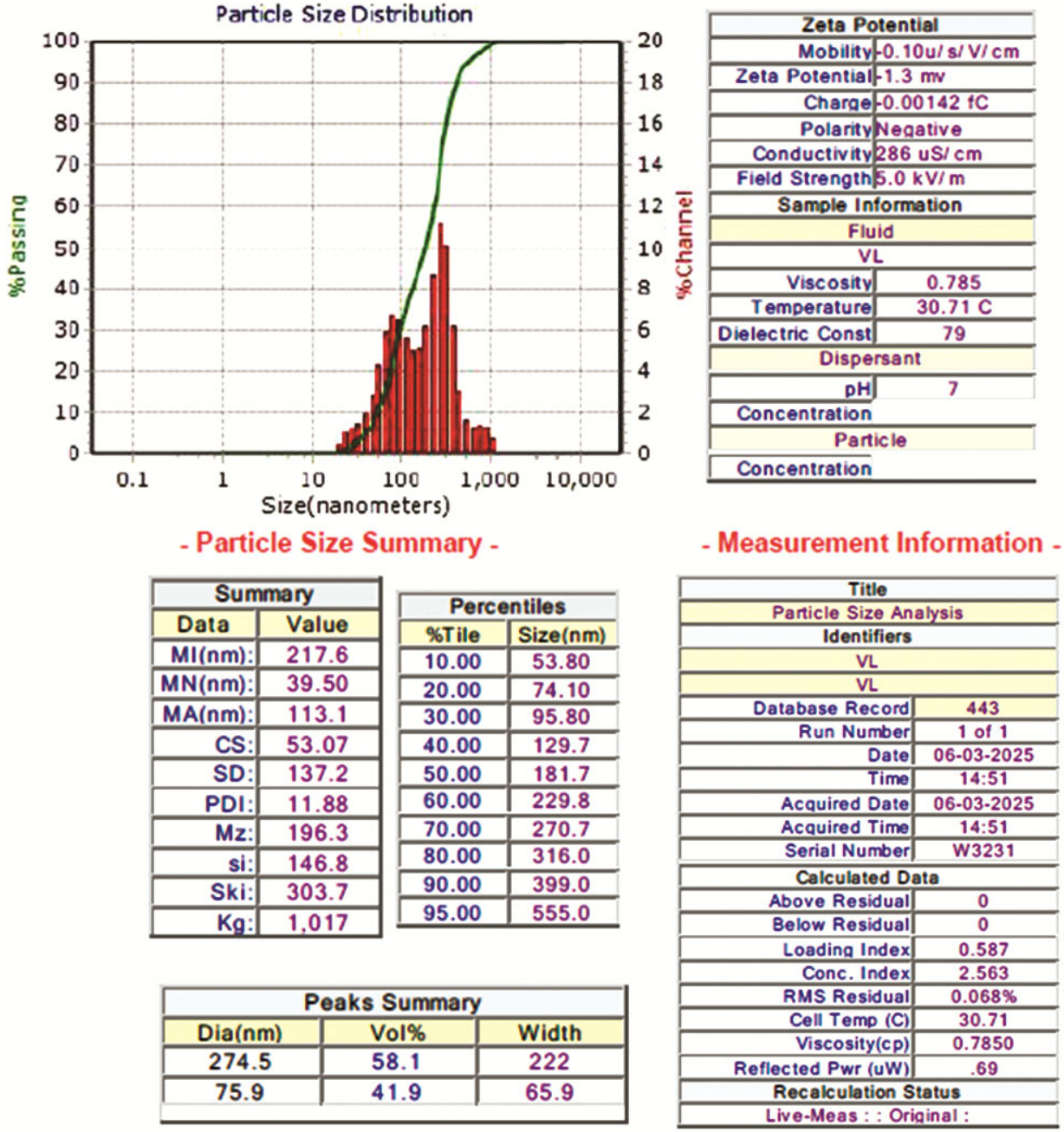

Fig. 6 — DLS particle size analysis of green-synthesised silver nanoparticles VL.

41.9% of the total volume, while the secondary and dominant peak was recorded at 274.5 nm, accounting for 58.1% of the volume. These values represent the hydrodynamic diameter, which is typically larger than the core size due to the hydration shell and surface-bound phytochemicals. The mean particle size (MI) was approximately 217.6 nm, with a SD of 137.2 nm and a PDI of 0.188, indicating a moderately monodisperse system.

Anti-inflammatory activity

LPS-induced MTT assay in RAW 264.7 cells

The anti-inflammatory efficacy of the biosynthesised AgVL and the crude *Vitex leucoxylon* (VL) extract was assessed using an MTT-based viability assay in LPS-stimulated RAW 264.7 macrophage cells. LPS treatment alone significantly reduced cell viability, indicating successful induction of inflammation. The OD value at 590 nm for untreated control cells was 0.869, whereas

Table 2 — Percentage recovery of inflammation of AgVL and VL extract at different concentrations

Extract			Conc µg/mL	OD at 590nm	% Recover
AgVL		Control	80 ng/mL	0.869	0
				0.241	72.27
	LPS 80ng/mL		80	0.433	50.17
			40	0.717	17.49
			20	0.653	24.86
			10	0.388	55.35
			5	0.341	60.76
			2.5	0.284	67.32
			1.25	0.258	70.31
VL		Control	80 ng/mL	0.881	0.00
				0.202	77.07
	LPS 80ng/mL		320	0.227	74.23
			160	0.277	68.56
			80	0.3787	57.01
			40	0.5945	32.52
			20	0.271	69.24
			10	0.257	70.83

LPS-treated cells showed a markedly reduced OD of 0.241, reflecting a 72.27% reduction in viability compared to the control.

***Vitex leucoxylon* treatment**

The plant extract alone (VL) demonstrated decent anti-inflammatory activity. Treatment with 10 µg/mL of VL showed the highest recovery of 70.83%, followed by 20 µg/mL (69.24%) and 160 µg/mL (68.56%). However, recovery rates were generally lower at both the highest (320 µg/mL: 74.23%) and lowest (VL + LPS: 77.07%) doses compared to AgVL (Table 2). These findings suggest that while VL possesses inherent anti-inflammatory properties, the nanoparticle formulation (AgVL) enhances the bioavailability and efficacy, particularly at lower concentrations. This biphasic pattern suggests an optimal therapeutic window around 40 µg/mL, beyond which the efficacy diminishes potentially due to saturation effects, feedback inhibition, or cytotoxicity at elevated concentrations. These findings reinforce the potency of the VL extract at moderate doses in mitigating inflammation.

AgVL treatment

At higher concentrations, a decline in cell recovery was observed, with viability decreasing from 55.35% at 10 µg/mL to 50.17% at 80 µg/mL, suggesting a dose-dependent cytotoxic effect at elevated doses (Table 2). These findings indicate that while AgVL exhibits potent anti-inflammatory activity at lower concentrations, its therapeutic window may narrow at higher exposures.

Nitric oxide (NO) assay

The anti-inflammatory potential of silver nanoparticles synthesised from *Vitex leucoxylon* (AgVL) and the crude plant extract (VL) was further evaluated by quantifying nitric oxide (NO) production in LPS-stimulated RAW 264.7 macrophages. NO is a key pro-inflammatory mediator produced by activated macrophages, and its suppression is indicative of anti-inflammatory efficacy.

AgVL treatment

LPS stimulation led to an increase in NO levels, from 0.922 µg/mL (control) to 2.574 µg/mL, indicating successful induction of an inflammatory state. Treatment with AgVL resulted in a dose-dependent decrease in NO production. At the lowest concentration of 2.5 µg/mL, NO levels reduced to 2.089 µg/mL, while a notable reduction was observed at 5 µg/mL (1.578 µg/mL) and 10 µg/mL (1.166 µg/mL). The maximum inhibition was recorded at 40 µg/mL, where NO concentration declined to 0.825 µg/mL, nearly restoring baseline levels (Fig. 7). These findings suggest that AgVL effectively suppressed NO production, particularly at 20–40 µg/mL, demonstrating strong anti-inflammatory potential.

VL treatment

In the case of crude VL extract, LPS-stimulated cells exhibited an NO level of 2.718 µg/mL, slightly higher than that observed in the AgVL group. Treatment with VL also led to a concentration-

dependent reduction in NO levels, but to a lesser extent compared to AgVL. NO concentrations decreased to 2.248 µg/mL at 10 µg/mL, 2.065 µg/mL at 20 µg/mL, and 1.850 µg/mL at 40 µg/mL (Fig. 8). The most substantial reduction was seen at 160 µg/mL, where NO concentration fell to 1.639 µg/mL—still notably higher than that achieved by AgVL at much lower concentrations.

Comparison

The crude *Vitex leucoxylon* extract (VL) also exhibited measurable anti-inflammatory effects, with

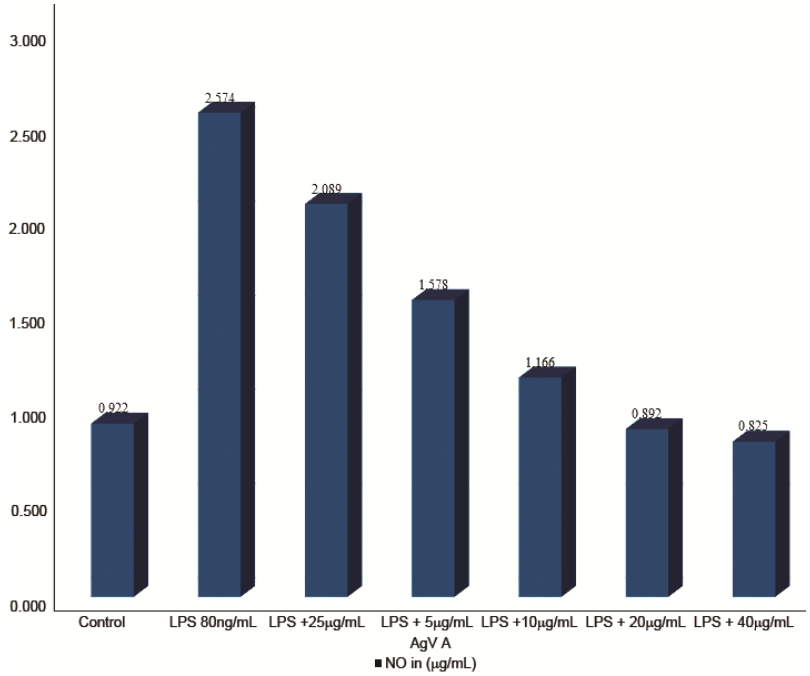

Fig. 7 — Quantified Nitric oxide after treatment AgVL against RAW 264.7 cell line.

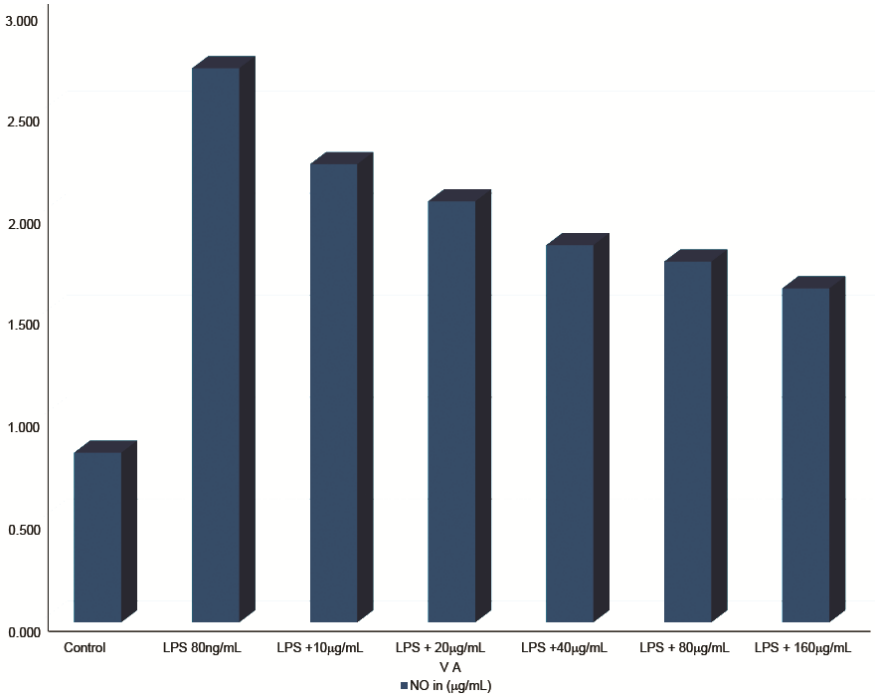

Fig. 8 — Quantified Nitric oxide after treatment VL against RAW 264.7 cell line.

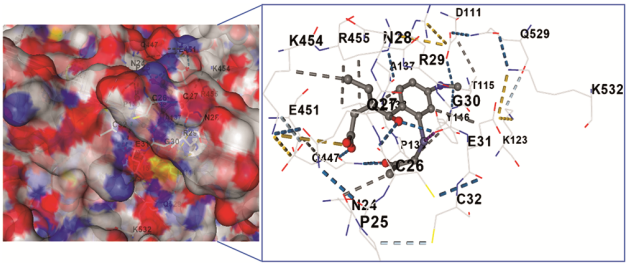

Fig. 9 — Molecular interaction analysis of the Zn-based ligand (proxy of Ag-based ligand) within Cavity C2 of COX-2 (PDB ID: 3LN1).

70.83% cell recovery at 10 µg/mL and a reduction of NO concentration to 1.850 µg/mL at 40 µg/mL. However, AgVL nanoparticles demonstrated superior activity at substantially lower concentrations, achieving 70.31% recovery at only 1.25 µg/mL and reducing NO to 0.825 µg/mL at 40 µg/mL. These findings indicate that while the crude extract possesses intrinsic activity, nanoparticle formulation markedly enhances potency and efficacy.

Docking results and binding affinity evaluation

The docking analysis revealed five potential binding cavities (C1–C5) on the COX-2 protein structure. Each cavity was evaluated for its binding affinity with the zinc-based ligand that served as a proxy for silver nanoparticles. Among the five cavities, Cavity 2 (C2) exhibited the strongest binding affinity, with a binding score of –8.3 kcal/mol, indicating a highly favourable interaction with the ligand. The ligand was deeply embedded in a pocket formed by multiple polar and charged residues, contributing to its strong binding potential. Key residues involved in direct interaction included Q27, N28, R29, G30, E31, and C26, which formed hydrogen bonds, polar contacts, and potential metal coordination with the Zn center. The interaction map also showed additional support from residues such as E451, R455, K454, and Q529, stabilising the complex via salt bridges and electrostatic interactions (Fig. 9). The ligand formed a hydrogen bond network notably with E31, N28, and Q27, while C26 and P25 appeared to be involved in hydrophobic or van der Waals interactions. The presence of positively charged residues like R29, K454, and R455 near the Zn center might have favoured electrostatic stabilisation of the metal-phytochemical complex. This dense clustering of interactive residues suggested a highly favourable environment for metal coordination and ligand anchoring.

Table 3 — Binding energies of the Zn-based ligand (proxy of Ag-based ligand) within Cavity C2-C5 of COX-2 (PDB ID: 3LN1)

Cavity	Binding score
C1	-7.1
C2	-8.3
C3	-7.8
C4	-8.2
C5	-8.2

This was closely followed by cavities 4 and 5 (C4 and C5), both of which showed binding energies of –8.2 kcal/mol, suggesting similar potential for effective ligand binding. Cavity 3 (C3) demonstrated a slightly lower but still significant binding score of –7.8 kcal/mol, while cavity 1 (C1) presented the weakest binding affinity among the five, with a docking score of –7.1 kcal/mol (Table 3). Despite being the least favorable, the binding score in C1 still indicated a moderate level of interaction.

These results suggested that the Zn-based ligand had a preferential binding profile toward multiple active or allosteric sites on the COX-2 protein. The consistently high binding affinity observed in C2, C4, and C5 supported the hypothesis that plant-extract-mediated metal nanoparticles may serve as effective modulators of COX-2 activity. Further analysis of the amino acid residues involved in each cavity is required to determine the specificity and nature of molecular interactions, particularly in C2, where the strongest binding was observed.

Because AutoDock Vina does not directly support metallic nanoparticles, a Zn-based dummy metal approach was used to approximate the AgNP core, following the AutoDock4Zn protocol. This dummy metal was incorporated into a simple organic scaffold derived from dominant phytochemical structures (e.g., flavonoids, phenolic acids), thereby representing a phytochemical-metallic complex rather than a single Ag atom or large nanoparticle cluster. This strategy enabled the modeling of biologically relevant interactions between nanoparticle-associated phytochemicals and the COX-2 active site.

Discussion

The present study demonstrates the successful green synthesis of AgNPs using *Vitex leucoxylon* leaf extracts, characterized by UV–Visible spectroscopy, FTIR, XRD, SEM, and DLS analysis. The synthesised AgNPs showed notable anti-inflammatory activity,

confirmed through both *in vitro* protein denaturation inhibition and molecular docking analysis. These findings are consistent with, and in several respects extend, the current understanding of synthesized AgNPs and their biomedical applications.

The UV–Vis absorption peak observed around 400 nm confirms the SPR characteristic of AgNPs, aligning well with previous reports using other plant extracts such as *Azadirachta indica* and *Ocimum sanctum,* which reported SPR peaks between 375–452 nm[29–31]. Interestingly, Zargar *et al*. also reported the absorption peak around 422 nm from the *Vitex Negundo*-based silver nanoparticle[32]. This substantiates that the phytoconstituents in *V. leucoxylon* are capable of both reducing and stabilising AgNPs. FTIR spectra revealed peaks corresponding to O–H, N–H, and C=O functional groups, suggesting the involvement of flavonoids, alkaloids, and phenolic compounds in capping and reducing Ag^+ ions. This is in alignment with the findings of Alex *et al*., where bioactive compounds from Ocimum species were identified as key functional moieties in nanoparticle synthesis[33].

XRD patterns confirmed the FCC crystalline nature of the synthesised AgNPs, with an average crystalline size estimated at (41.9-66.4 nm). This is similar to the size reported in *V. trifolia*-mediated AgNPs (20 nm)[34]. However, our reported size is slightly larger than the average sizes reported in *Ocimum canum*-mediated AgNPs (15.72 nm)[15] likely due to differences in extract concentration, reaction kinetics, and phytochemical profile.

The bimodal size distribution observed in DLS, with peaks at ~75.9 nm and ~274.5 nm, suggests the coexistence of two nanoparticle populations. The smaller fraction likely facilitates effective cellular uptake and contributes to the anti-inflammatory efficacy, whereas the larger fraction may represent phytochemical-coated aggregates or secondary clusters. Such heterogeneity can influence biological behaviour: Smaller particles typically enhance bioactivity, while larger clusters may reduce toxicity by limiting intracellular accumulation. Although our *in vitro* results showed favourable biological activity without overt cytotoxicity, further *in vivo* studies are warranted to evaluate how this size distribution impacts biodistribution, clearance, and long-term safety.

The *in vitro* anti-inflammatory assay showed substantial inhibition of protein denaturation (up to 70.31% recovery at 1.25ug/mL), aligning the earlier studies involving biosynthesised FeNPs from *V. trifolia* leaf (80% inhibition)[35]. This enhanced activity can be attributed to the synergistic action of AgNPs with phytochemicals in *V. leucoxylon*, which may act on multiple inflammatory pathways. Similar trends were reported by Nahari *et al*., where *V. leucoxylon* FeNPs showed a 10-15% higher inhibition than the extract alone[17]. The data clearly indicate that AgVL demonstrated superior NO inhibition at lower concentrations compared to the crude extract. For instance, AgVL at 20 µg/mL brought NO levels down to 0.892 µg/mL close to the baseline whereas VL required 160 µg/mL to achieve a less significant reduction to 1.639 µg/mL. This enhanced activity of AgVL is likely due to the improved bioavailability, targeted cellular interaction, and sustained release of phytoconstituents in nanoparticle form. These results reinforce the hypothesis that green synthesised AgNPs potentiate the anti-inflammatory action of the parent plant compound. In this study, the anti-inflammatory efficacy of AgVL nanoparticles was compared with the crude extract but not with standard NSAIDs such as indomethacin or diclofenac. Literature reports indicate that biosynthesised AgNPs can exert inhibitory effects on inflammatory mediators comparable to or slightly lower than conventional NSAIDs, depending on concentration and formulation[36]. Although our findings demonstrate significant suppression of nitric oxide and improved cell recovery relative to the extract, future studies should incorporate standard anti-inflammatory drugs as reference controls to establish the relative potency of AgVL nanoparticles in a clinically relevant context.

Further, *in silico* docking of AgVL nanoparticle against COX-2 revealed strong binding affinities (−8.3 kcal/mol). This suggests that *V. leucoxylon*-derived molecules not only assist in nanoparticle synthesis but also contribute to the observed anti-inflammatory effects. It is important to note that molecular docking simulations of nanoparticles with proteins are inherently limited, as most docking algorithms are optimised for small molecules rather than particulate systems. In this study, the Zn-dummy atom approach was used as a proxy to mimic the core of AgNPs, with an attached phytochemical scaffold representing the surface-bound biomolecules. Therefore, the docking results are interpreted as

indicative of the potential interactions between phytochemical-capped AgNP surfaces and COX-2 residues, rather than a literal simulation of nanoparticle binding. These computational insights, when viewed alongside the experimental NO inhibition results, suggest a plausible mechanism of anti-inflammatory activity but require further *in vivo* validation for full physiological relevance.

Beyond confirming the feasibility of green synthesis, this work advances the field of green nanotechnology by introducing *V. leucoxylon* as a novel biogenic source capable of producing stable, crystalline AgNPs through an eco-friendly route. Unlike conventional chemical methods, the process avoids hazardous reagents, ensuring sustainability and safety. Furthermore, the integration of *in vitro* and *in silico* approaches advances the current knowledge of anti-inflammatory therapeutics by establishing mechanistic insights into COX-2 inhibition and demonstrating the superior efficacy of AgNPs compared to the crude extract. This synergistic use of green synthesis and biological validation highlights the translational potential of nanophytomedicine.

Despite promising results, this study has some limitations. First, the anti-inflammatory potential was evaluated using a simplified *in vitro* cell line assay and *in silico* docking, which may not fully represent the complexity of inflammatory pathways *in vivo*. Second, the study did not assess cytotoxicity on mammalian cell lines or primary human cells, which limits understanding of the formulation's safety profile. While SEM, XRD, FTIR, and DLS together provided strong evidence for successful AgNP synthesis, future studies incorporating TEM and EDS analyses will be valuable to confirm fine structural features and elemental mapping at the nanoscale. A further limitation is the absence of complementary techniques such as transmission electron microscopy (TEM) and energy-dispersive X-ray spectroscopy (EDS), which could provide higher-resolution insights into nanoparticle morphology and definitive elemental composition. Third, the precise identification and quantification of bioactive phytoconstituents responsible for synthesis and activity were not conducted using HPLC or LC-MS/GC-MS. Finally, pharmacokinetics, clearance, biodistribution, and long-term stability in biological fluids remain unaddressed and warrant further investigation in animal models.

Conclusion

In this study, silver nanoparticles were successfully synthesised using *V. leucoxylon* leaf extract via a green and eco-friendly route, fulfilling our objective of evaluating their potential as anti-inflammatory agents. The nanoparticles were confirmed by UV–Vis, FTIR, SEM, XRD, and DLS analyses to be crystalline, spherical, and capped with phytochemicals. Biological assays demonstrated that AgVL nanoparticles significantly suppressed nitric oxide production and improved cell recovery in LPS-stimulated RAW 264.7 macrophages, showing greater potency than the crude extract at lower concentrations. *In silico* docking studies, performed using a phytochemical-metallic proxy model, further supported COX-2 inhibition as a plausible mechanism of action. Collectively, these findings highlight the promise of *V. leucoxylon*-mediated AgNPs as potential green anti-inflammatory candidates. Nonetheless, *in vivo* studies addressing pharmacokinetics, biodistribution, stability, and safety will be essential to confirm their translational applicability.

Conflict of Interest

The authors declared no conflict of interest.

References

1 Chen L, Deng H, Cui H, Fang J, Zuo Z & Deng J. Inflammatory responses and inflammation-associated diseases in organs. *Oncotarget* 9 (2018) 7204.

2 Jomova K, Alomar SY, Valko R, Liska J, Nepovimova E & Kuca K. Flavonoids and their role in oxidative stress, inflammation, and human diseases. *Chem Biol Interact* 413 (2025) 111489.

3 WHO. Noncommunicable diseases. WHO (2024) Available from: https://www.who.int/news-room/fact-sheets/ detail/non communicable-diseases [Accessed 31 May 2025].

4 Bindu S, Mazumder S & Bandyopadhyay U. Non-steroidal anti-inflammatory drugs (NSAIDs) and organ damage: A current perspective. *Biochem Pharmacol* 180 (2020) 1.

5 Amponsah SK, Tagoe B, Adams I & Bugyei KA. Efficacy and safety profile of corticosteroids and non-steroidal anti-inflammatory drugs in COVID-19 management: A narrative review. *Front Pharmacol* 13 (2022) 1.

6 Elzein B. Nano Revolution: Tiny tech, big impact: How nanotechnology is driving SDGs progress. *Heliyon* 10 (2024) e31393.

7 Ahmad A, Haneef M, Ahmad N, Kamal A, Jaswani S & Khan F. Biological synthesis of silver nanoparticles and their medical applications (Review). *World Acad Sci J* 6 (2024) 1.

8 Meher A, Tandi A, Moharana S, Chakroborty S, Mohapatra SS & Mondal A. Silver nanoparticle for biomedical applications: A review. *Hybrid Adv* 6 (2024) 100184.

9 Jain K, Takuli A, Gupta TK & Gupta D. Rethinking Nanoparticle Synthesis: A Sustainable Approach vs. Traditional Methods. *Chem Asian J* 19 (2024) 445.

10 Shayo GM, Elimbinzi E & Shao GN. Preparation methods, applications, toxicity and mechanisms of silver nanoparticles as bactericidal agent and superiority of green synthesis method. *Heliyon* 10 (2024) e36539.

11 Thatyana M, Dube NP, Kemboi D, Manicum ALE, Mokgalaka-Fleischmann NS & Tembu JV. Advances in Phytonanotechnology: A Plant-Mediated Green Synthesis of Metal Nanoparticles Using Phyllanthus Plant Extracts and Their Antimicrobial and Anticancer Applications. *Nanomaterials* 13 (2023) 1.

12 Bao Y, He J, Song K, Guo J, Zhou X & Liu S. Plant-Extract-Mediated Synthesis of Metal Nanoparticles. *J Chem* 2021 (2021) 1.

13 Makwana HG, Ravishankar B, Shukla VJ, Bhaskaran Nair R, Vijayan NP & Sasikala CK. General pharmacology of Vitex leucoxylon Linn leaves. *Indian J Physiol Pharmacol* 38 (1994) 95.

14 Aditya K & Ravi Kumar A. Phytochemical evaluation of Vitex leuocoxylon, Vitex negundo and Vitex trifolia. *J Res Pharm Biotechnol* 5674 (2014) 2320.

15 Yadav CK, Chaube A, Thapa S, Palikhey A, Shrestha L & Kandel K. In-Vitro Anti-Diabetic Activity and Phytochemical Screening of Ethanolic extract of Calotropis gigantea (Linn). *J Univ Coll Med Sci* 11 (2023) 50.

16 Pandey B, Thapa S, Kaundinnyayana A & Panta S. Hepatoprotective effects of Juglans regia on carbon tetrachloride-induced hepatotoxicity: In silico/in vivo approach. *Food Sci Nutr* 12 (2024) 6482.

17 Liaqat N, Jahan N, Khalil-ur-Rahman, Anwar T & Qureshi H. Green synthesized silver nanoparticles: Optimization, characterization, antimicrobial activity, and cytotoxicity study by hemolysis assay. *Front Chem* 10 (2022) 1.

18 Nahari MH, Al Ali A, Asiri A, Mahnashi MH, Shaikh IA & Shettar AK. Green Synthesis and Characterization of Iron Nanoparticles Synthesized from Aqueous Leaf Extract of Vitex leucoxylon and Its Biomedical Applications. *Nanomaterials* 12 (2022) 1.

19 Tian Y, Zhou S, Takeda R, Okazaki K, Sekita M & Sakamoto K. Anti-inflammatory activities of amber extract in lipopolysaccharide-induced RAW 264.7 macrophages. *Biomed Pharmacother* 141 (2021) 111854.

20 Lamichhane G, Pandeya PR, Lamichhane R, Yun HD, Shrivastava AK & Cheon JY. Evaluation of anti-inflammatory potential of extract, fractions and major compounds of Ponciri Fructus in LPS-induced RAW 264.7 cells. *Curr Res Biotechnol* 6 (2023) 100138.

21 Wang Z, Guan Y, Yang R, Li J, Wang J & Jia AQ. Anti-inflammatory activity of 3-cinnamoyltribuloside and its metabolomic analysis in LPS-activated RAW 264.7 cells. *BMC Complement Med Ther* 20 (2020) 1.

22 Alfaiz FA. Anti-Inflammatory Activity Potential of Arglabin in LPS-Stimulated RAW 264.7 Macrophages. *Int J Pharm Investig* 15 (2024) 237.

23 Bryan NS & Grisham MB. Methods to detect nitric oxide and its metabolites in biological samples. *Free Radic Biol Med* 43 (2007) 645.

24 Ahsan A, Farooq MA & Perveen A. Green Synthesis of Silver Nanoparticles Using Characterization and In Vitro Therapeutic Evaluation. *Molecules* 25 (2020) 1.

25 Gaddam SA, Kotakadi VS, Subramanyam GK, Penchalaneni J, Challagundla VN & Dvr SG. Multifaceted phytogenic silver nanoparticles by an insectivorous plant Drosera spatulata Labill var. bakoensis and its potential therapeutic applications. *Sci Rep* 11 (2021) 1.

26 Santos-Martins D, Forli S, Ramos MJ & Olson AJ. AutoDock4Zn: An improved AutoDock force field for small-molecule docking to zinc metalloproteins. *J Chem Inf Model* 54 (2014) 2371.

27 Gote S, Thapa S, Dubey S, Nargund SL & Biradar MS. Computational investigation of quinazoline derivatives as Keap1 inhibitors for Alzheimer's disease. *Inform Med Unlocked* 41 (2023) 1.

28 Jini D, Sharmila S, Anitha A, Pandian M & Rajapaksha RMH. In vitro and in silico studies of silver nanoparticles (AgNPs) from Allium sativum against diabetes. *Sci Rep* 12 (2022) 1.

29 Huda Abd Kadir N, Khan AA, Kumaresan T, Khan AU & Alam M. The impact of pumpkin seed-derived silver nanoparticles on corrosion and cytotoxicity: a molecular docking study of the simulated AgNPs. *Green Chem Lett Rev* 17 (2024) 1.

30 Liu Y, Grimm M, Dai WT, Hou MC, Xiao ZX & Cao Y. CB-Dock: a web server for cavity detection-guided protein–ligand blind docking. *Acta Pharmacol Sin* 41 (2020) 138.

31 Kumari SA, Patlolla AK & Madhusudhanachary P. Biosynthesis of Silver Nanoparticles Using Azadirachta indica and Their Antioxidant and Anticancer Effects in Cell Lines. *Micromachines* 13 (2022) 1.

32 Gautam D, Dolma KG, Khandelwal B, Gupta M, Singh M & Mahboob T. Green synthesis of silver nanoparticles using Ocimum sanctum Linn. and its antibacterial activity against multidrug resistant Acinetobacter baumannii. *PeerJ* 11 (2023) 1.

33 Roy P, Das B, Mohanty A & Mohapatra S. Green synthesis of silver nanoparticles using Azadirachta indica leaf extract and its antimicrobial study. *Appl Nanosci* 7 (2017) 843.

34 Zargar M, Hamid AA, Bakar FA, Shamsudin MN, Shameli K & Jahanshiri F. Green synthesis and antibacterial effect of silver nanoparticles using Vitex negundo L. *Molecules* 16 (2011) 6667.

35 Alex AM, Subburaman S, Chauhan S, Ahuja V, Abdi G & Tarighat MA. Green synthesis of silver nanoparticle prepared with Ocimum species and assessment of anticancer potential. *Sci Rep* 14 (2024) 1.

36 Chinnasamy R, Chinnaperumal K, Arumugam P, Natarajan M, Govindasamy B & Jogikalmat K. Phyto-fabrication of AgNPs using leaf extract of Vitex trifolia: potential to antibacterial, antioxidant, dye degradation, and their evaluation of non-toxicity to Chlorella vulgaris. *Biomass Convers Biorefinery* 14 (2024) 14903.